A Reduced Order Model for Permeability Fields Using Singular Value Decomposition (SVD)

B. Lashore[a,*], K. Christou[a], J.L.M.A. Gomes[a]

[a]*Mechanics of Fluids, Soils & Structures Research Group*
School of Engineering, University of Aberdeen, UK

Abstract

Representation of heterogeneous properties (*i.e.,* permeability in this case) within a large system, is a challenge that cuts across many industries that deal with flows in porous media. This is because it is impossible to obtain the value of permeability at every point in realistic domains. And, even if this was possible, it would be extremely challenging to get the computing resources to make use of all available data values. This challenge gave birth to upscaling, a model order reduction method.

In this paper, a SVD-based method was developed to reduce the order of porous media permeability field (*i.e.,* upscale). This method was compared to traditional industry-standard upscaling techniques (*e.g.,* arithmetic and harmonic averaging) and to a stochastic-based (probability density function, PDF) method of upscaling, to highlight its benefits/performance. It was shown that the SVD upscaling technique retained the heterogenous nature of the BaseCase (*i.e.,* high-resolution configuration). Additionally, the SVD upscaling technique did not require *a priori* understanding of similar permeability blocks within the existing domain.

Keywords: Singular Value Decomposition (SVD), Upscaling, Model Order Reduction (MOR), Principal Component Spaces, Permeability field, Heterogeneity

*Corresponding author.
Email address: lashorebabatunde@yahoo.com (B. Lashore)

1. Introduction

Naturally occuring rock formations are inherently heterogeneous, which means that rock properties such as permeability, pore spaces (*i.e.,* porosity) and pore throat vary spatially at different length scales. Heterogeneity of rock formations is relevant in calculations of transport and storage of fluids in porous media (*i.e.,* multiphase flow in subsurface rocks). Therefore, the representation of such heterogeneous properties is of great importance to oil and gas (*i.e.,* reservoir management), carbon capture and storage (CCS, *i.e.,* CO_2 transportation and storage in subsurface rocks) and waste management (*i.e.,* remediation of contaminated soil).

In essence, rock heterogeneity makes it impossible to obtain reliable and accurate spatial information about geological properties throughout the domain (*i.e.,* uncertainty problem). Additionally, due to limitations in computing resources, it is neither efficient nor possible to use exact values of geological properties at all spatial coordinates of the domain to perform fine-grid simulations (*i.e.,* scaling problem) [7, 24, 31]. This is particularly true for large geological domains which span several kilometres. It is possible to overcome these challenges by a family of techniques called *upscaling*. Upscaling techniques solve both uncertainty and scaling problems by replacing discrete geological and fluid properties of detailed high resolution domains with coarse descriptions (low resolution) of these properties [37].

Upscaling techniques which best preserve statistical properties and flow dynamics behaviour of the high resolution domain give the best representation of heterogeneous properties. There are several upscaling techniques which fall under different categories [18, 31, 36]. Traditional upscaling techniques are deterministic in nature, however over the last decade, techniques classed as stochastic have received great attention from academic and industrial porous media communities worldwide [17, 30, 38]. One of the reasons for this is because stochastic upscaling techniques are robust enough to handle multiphase flow in porous media and they are able to address scaling and uncertainity problems.

Upscaling is a term commonly used in the oil and gas sector and is often referred, throughout the applied mathematics and engineering communities, as a form of model order reduction (or reduced order models, MOR/ROM). Depending on the context in which MOR is used, it can simply be referred as dimensionality reduction. The definition of MOR also depends on the context it is being used, but it suffices to state that MOR captures the essen-

tial features of a system, structure or parameter [34]. This implies that an original system exists with more detailed information. Figure 1 presents an interpretation of MOR concept in which a graphical representation of a rabbit is reconstructed with a reduced number of facets (rhs of this illustration).

Schilders [34] provided a historical perspective on the development of Model Order Reduction, from the work of Fourier in 1807 which approximated a function with a few trigonometric terms, to the work of Odabasioglu et al. [26] in 1998 which introduced Passive Reduced-order Interconnect Macromodeling Algorithm (PRIMA). Truncated Balanced Realization is another MOR method developed by Moore [25], which introduced the principal component analysis [20] and Golub and Reinsch's [15] algorithm for solving singular value decomposition (SVD). Hankel-norm reduction [14] and Proper Orthogonal Decomposition [35] are also MOR methods discussed in the references published in 1984 and 1987, respectively. The asymptotic waveform evaluation (AWE) [29] was the first MOR method based on Krylov subspace technique, this method was followed by Pade-via-Lanczos method [12] and the PRIMA. In this work, upscaling is performed by SVD in principal component spaces.

This work focuses on reducing the order of permeability distribution in porous media flow simulations. Section 2 introduces the mathematical model used to describe the relevant physics for multi-fluid flow through porous media and highlights the relevance of the permeability field. The mathematical model is discretised by a novel high-order accurate control volume finite element method (CVFEM) [16] which couples both the fine resolution and upscaled representation of the permeability field. Pre-processing statistical properties and post-simulation multiphase flow behaviour are investigated to assess the various upscaling techniques used.

Four upscaling techniques are investigated in this work, arithmetic and harmonic means are used to obtain the first two upscaled representation and these two are classed as deterministic techniques. The third is a randomly generated permeability field with Gaussian distribution, prescribed by a probability density function (PDF) which was obtained from a domain discretised with high-resolution mesh with known permeability distribution (*i.e.,* base case). The fourth upscaling technique is the crux of this research, it introduces singular value decomposition (SVD) as a method of upscaling using the concept of principal component space to reduce the order of the permeability distribution.

In Section 4, fundamental mathematics of SVD and associated properties are presented. Then, the concept of spaces is explained to give the reader the understanding necessary to appreciate the transformations and projections involved in this work. Finally, Section 4 describes model order space reduction for the permeability field within the principal component space. Section 5 starts by describing the high resolution (*i.e.,* base case) on which the four upscaling techniques are applied to. A brief summary of the preprocessing step for each of the models is also presented. Section 6 provides the results and further discussion on the results of the simulations, it also gives further interpretation to the result obtained from the SVD upscaling technique. Finally, Conclusions are drawn in Section 7.

2. Multi-Fluid Flow Model

In this work, a novel control volume finite element method (CVFEM) formulation is used to discretise and solve the set of multi-fluid flow equations. Continuity equations are embedded into the pressure equation to enforce mass conservation and the exact force balance (extended Darcy equations). The numerical formulation employs an implicit algorithm with respect to time which is less restrictive than the traditional industry-standard implicit-pressure-explicit-saturation (IMPES) scheme [3, 13].

The formulation used in this work uses a dual consistent CVFEM representation which is embedded in novel families of triangular and tetrahedral finite element-pairs, $\mathrm{P}_n\mathrm{DG}\text{-}\mathrm{P}_m$ and $\mathrm{P}_n\mathrm{DG}\text{-}\mathrm{P}_m\mathrm{DG}$. In this element-pairs velocity is represented by n^{th}-order polynomials that are discontinuous across elements, while pressure is represented by m^{th}-order polynomials that may be either continuous ($\mathrm{P}_n\mathrm{DG}\text{-}\mathrm{P}_m$) or discontinuous ($\mathrm{P}_n\mathrm{DG}\text{-}\mathrm{P}_m\mathrm{DG}$) across elements. Most properties of $\mathrm{P}_n\mathrm{DG}\text{-}\mathrm{P}_m\mathrm{DG}$ element-pairs are similar to those in the $\mathrm{P}_n\mathrm{DG}\text{-}\mathrm{P}_m$ element-pairs but allows a representation in which pressure, saturation and other solution variables (*e.g.,* temperature, concentrations etc) are discontinuous across finite element boundaries [32, 1].

Immiscible multi-fluid flows in porous media may be represented by the extended Darcy equation,

$$\mathbf{q}_\alpha = \mathbf{u}_\alpha S_\alpha = -\frac{\mathcal{K}_{r_\alpha}\mathbf{K}}{\mu_\alpha}\left(\nabla p_\alpha - \mathbf{s}_{u\alpha}\right), \tag{1}$$

where α designates a phase, $\mathbf{q}_\alpha$ is the α-th phase Darcy velocity and $\mathbf{u}_\alpha$ is the saturation-weighted Darcy velocity. μ_α, p_α, ρ_α, and $\mathbf{s}_{u_\alpha}$ are the phase

dynamic viscosity, pressure, density and source term, which may include gravity and/or capillarity, respectively. $\mathcal{K}_{r_\alpha}(S_\alpha)$ is the phase relative permeability, which is a function of the phase saturation $S_\alpha(\mathbf{r}, t)$, which in turn is a function of the vector position $\mathbf{r}$, and time, t.

In addition to the extended Darcy equation (Eqn. 1), saturation conservative equations,

$$\phi \frac{\partial S_\alpha}{\partial t} + \nabla \cdot (\mathbf{u}_\alpha S_\alpha) = s_{cty,\alpha}, \tag{2}$$

are discretised in space with CV basis functions, and in time with the θ-method [27]. In Eqn. 2, ϕ is the porosity and s_{cty} is a source term.

The discretised saturation and Darcy equations are solved using a multigrid-like approach as described by Pavlidis et al. [28]. The numerical formulation is fully described by Gomes et al. [16] (see also [33, 1]). These numerical methods are embedded in the next-generation flow simulator Fluidity/ICFERST model software[1] (a full description of the model can be found in [22, 16]).

Finally, $\mathbf{K}(\mathbf{r})$, the focus of this work, is the absolute permeability tensor of the porous medium and it is a function of the vector position $\mathbf{r}$. $\mathbf{K}$ is prescribed in the system of governing conservative equations, *i.e.,* it is an indepedent input variable. Since $\mathbf{K}$ is a petrophysical rock property that varies spatially, it cannot be determined at every spatial coordinate. And, even if this information is available at every spatial coordinate, it would require immense computer resources to process during flow simulations. This is the reason upscaling is required for processing permeability variables. Upscaling can be performed from the continuum scale, across the micro scale (mm), local scale and meso scale (m) to the field scale (km)[19]. The upscaling discussed here is from the micro scale also known as the Darcy scale.

3. Brief Overview of Upscaling

Section 1 briefly introduced the rational behind upscaling. Upscaling methods replace discrete geological and fluid properties of detailed high resolution domains with coarse descriptions (low resolution) of these properties

[1] http://multifluids.github.io

[37]. This subject of upscaling heterogenous properties has interested industries (*i.e.,* oil and gas, CCS and waste management) as well as the academic community for over 7 decades.

Those interested in large-scale reservoirs or ground water generally take a two-stage geostatistical approach. In the first stage, information from seismic data, well data and analogous outcrops is used to model the large scale heterogeneities associated with facies. In the second stage, statistical models such as continuous multi-variate Gaussian field is used to model the rock properties of the facies [11]. In addition to seismic and well data used in the previous stage, core data can be used as a sources of information for the statistical properties used to determine the random field in this stage.

Several studies were carried out on the upscaling of permeability fields [8, 11, 18, 23, 21, 37, 39, 40]. Cardwell and Parsons [6] investigated arithmetic and weighted averages as upscaling techniques for calculating a single equivalent permeability for oil reservoirs with varying permeabilities. The general conclusion reached from this study was that the equivalent permeability lies between the harmonic and the arithmetic average.

Yeo and Zimmerman [40] discussed the accuracy of renormalization method for upscaling 2D hydraulic conductivity fields for two cases. Both cases employed the 4-quadrant model (see Section 5.1 for details) set-up. The first case had low permeablitity in all the blocks except the bottom right block which had high permeability, while the second case employed the checkboard style described in Section 5.1. Different conductivity ratios were also investigated for the two cases. The conclusion drawn was that renormalization worked fairly well for the first case, but very poorly for the second case.

Renard and de Marsily [31] provided a comprehensive review of the various techniques for upscaling. They found out that the techniques classed broadly under deterministic, stochastic and heuristic complemented each other rather than antagonising each other. Renard and de Marsily [31] then recommended that it is better to select a technique which provides block permeabilities instead of one which provides uniform effective permeability.

Christie and Blunt [8] provided 2 sets of problems to compare the upscaling and upgridding techniques of different simulators. The paper does not describe in any detail the upscaling techniques used by the different simulators, but it provides a complete dataset for running simulations.

4. Singular Value Decomposition (SVD) and Application for Reducing the Order of Permeability Fields

4.1. A Brief Introduction to SVD

Given a matrix $\mathbf{A} \in \mathcal{R}^{m \times n}$, the singular value decomposition (SVD) is a method for factorizing $\mathbf{A}$, such that,

$$\mathbf{A} = \mathbf{U}\mathbf{\Sigma}\mathbf{V}^{\intercal}. \tag{3}$$

where $\mathbf{U} = [\underline{u}_1, \underline{u}_2, \cdots, \underline{u}_m] \in \mathcal{R}^{m \times n}$ and $\mathbf{V} = [\underline{v}_1, \underline{v}_2, \cdots, \underline{v}_n] \in \mathcal{R}^{m \times n}$ are orthogonal but not necessarily the same. Σ is a diagonal matrix, *i.e.,*

$$\Sigma = \mathrm{diag}\left(\sigma_1, \sigma_2, \cdots, \sigma_r\right) \in \mathcal{R}^{m \times n},$$

and $r = \min\{m, n\}$ is the rank of $\mathbf{A}$, with $\sigma_1 \geq \sigma_2 \geq \cdots \sigma_r \geq 0$. The diagonal entries of Σ (*i.e.,* $\sigma_i, i = 1, r$) are called singular values of $\mathbf{A}$. If $\mathbf{A}$ is a square matrix then $\mathbf{U}$, Σ and $\mathbf{V}$ are also square matrices. Also, as $\mathbf{U}$ and $\mathbf{V}$ are orthogonals and unitary,

$$\mathbf{U}^{\intercal}\mathbf{U} = \mathbf{V}^{\intercal}\mathbf{V} = \mathbf{I}, \tag{4}$$

where $\mathbf{I}$ is an identity matrix. However, if $\mathbf{A}$ is an $m \times n$ matrix, $\mathbf{U}$ and $\mathbf{V}$ still remain as square matrices, albeit with different matricial sizes. $\mathbf{U}$ is an $m \times m$ while $\mathbf{V}$ is an $n \times n$. Another relevant property of $\mathbf{U}$ and $\mathbf{V}$ since they are square (irrespective of whether $\mathbf{A}$ is square or rectangular) is that

$$\mathbf{U}^{-1} = \mathbf{U}^{\intercal} \quad \text{and} \quad \mathbf{V}^{-1} = \mathbf{V}^{\intercal}, \tag{5}$$

and if $\mathbf{A}$ is an $m \times n$ matrix thus Σ is a diagonal $m \times n$ matrix.

For a rectangular matrix, the singular values fill the first r places on the main diagonal of Σ. The SVD benefits from the orthogonality of the columns in $\mathbf{U}$ and $\mathbf{V}$. The columns of $\mathbf{U}$ are known as the left singular vectors while the columns in $\mathbf{V}$ are known as the right singular vectors. A simple consideration of the benefit of the orthogonal factors, $\mathbf{U}$ and $\mathbf{V}$, is the ease with which they allow the inverse of the square matrix $\mathbf{A}$ to be calculated. This in turn makes it easy to solve the linear equations, $\mathbf{A}x = b$ with the SVD factorization,

$$\mathbf{U}\Sigma\mathbf{V}^{\intercal}x = b \implies x = \mathbf{V}\Sigma^{-1}\mathbf{U}^{\intercal}b, \tag{6}$$

with benefit of the orthogonal property already discussed.

4.2. Principal Component Spaces and Model Order Reduction for the permeability field

4.2.1. Understanding the permeability space

In 3D geometry, permeability is a tensor quantity, but for the purpose of the following explanation (and the remaining of this paper), a 2D geometry is assumed where permeability is a scalar quantity. Furthermore, the simulator prescribes the permeability field by assigning permeability values to the centre of element-pairs [9] which discretises the 2D simulation domain.

Permeability values assigned in the centre of the element/cell represents values of permeability for the associated element (*i.e.,* P_0DG element-pair). For simplicity, in the remaining part of this section, it will be assumed that the $2D$ geometry is discritized by a square grid with the value for each square element assigned in the centre of the element. This explanation allow one to easily visualize this permeability space because it is defined by the cartesian coordinates system.

The model order reduction for the permeability field discussed here is concerned with reducing the volume of permeability data within the permeability space. Consider for instance a small square which is discretized to contain four squares such that 4 data points are defined in the middle of the four squares. The permeability space of 4 can be reduced to a smaller value of 1 through an averaging process such as arithmetic, harmonic or geometric mean. This type of reduction is the focus of this paper, albeit the main focus of this paper is achieving this reduction through SVD in the principal component spaces.

4.2.2. Understanding the principal component spaces

Essentially, the existing permeability space is transformed through SVD to principal component spaces (PCS) where traditional principal component analysis is performed before interpolation is used to implement further data reduction in the principal component spaces. This reduced data in the PCS is then transformed back into the permeability space to obtain a reduced permeability space.

The PCS is more challenging to visualize because it usually consists of more than 3-D. An aid for visualizing the PCS is to write out the $\mathbf{U}$, $\mathbf{\Sigma}$ and $\mathbf{V}^\intercal$ matrices and consider the singular vectors (*i.e.,* columns in $\mathbf{U}$ and rows in $\mathbf{U}$) as separate PCS.

4.2.3. Model Order Reduction/Principal Component Space Reduction

For the SVD model order reduction of the permeability field, all the work is done in the principal component spaces. This can be completed in two steps: the first step is the principal component analysis (PCA) [20], where the singular values are examined and, based on a pre-defined criteria, z singular values are selected, starting from σ_1 and in a decreasing order, where $z \leq r$.

In the case with $z = r$, it can be assumed that step 1 has been ignored. However, when $z < r$, the first z columns of $\mathbf{U}$ and the first z rows of $\mathbf{V}^\intercal$ are extracted from $\mathbf{U}$ and $\mathbf{V}^\intercal$ to form new matrices $\mathbf{U_{new}}$ and $\mathbf{V^\intercal_{new}}$ respectively. The selected z singular values also form a new diagonal matrix, $\mathbf{\Sigma_{new}}$.

The second step involves interpolation within each singular vector (column in $\mathbf{U}$ and row in $\mathbf{V}^\intercal$) to reduce the data points in each column of $\mathbf{U}$ and in $\mathbf{V}^\intercal$. From this step, $\mathbf{U_{new2}}$ and $\mathbf{V^\intercal_{new2}}$ are obtained. The reduced permeability field is calculated by multiplying $\mathbf{U_{new2}}$, $\mathbf{\Sigma_{new}}$ and $\mathbf{V^\intercal_{new2}}$.

5. Model Description and Simulation Setup

5.1. Model Description

The BaseCase (*i.e.,* fine mesh resolution) model for the permeabiliy field builds on the 2×2 block, 4 quadrant model used initially by Cardwell and Parsons [6] and later by Yeo and Zimmerman [40] and Dawe and Grattoni [10]. These authors designed the permeability field for the quadrants in a checkerboard style which means that diagonally opposite blocks retained the same permeability values with one set of diagonally opposite blocks having a higher permeability value compared to the other set. Hence, one set of diagonally opposite blocks are referred to as high permeability blocks while the other set is referred to as low permeability blocks.

The BaseCase permeability model used here retains the checkerboard desgined used by the recently named authors. Albeit, the permeability dataset for each block in the set of diagonally opposite blocks have similar value (*i.e.,* not exactly the same as in the papers referred to), although one set can still be referred to as a set of high permeability blocks while the other set is referred to as a set of low permeability blocks. Furthermore, within each block, the permeability field varies within a pre-defined range and consists of 1600 permeability values. More details on the design of the permeability field for the BaseCase is available in section 5.1.1. Figures 3a and 3b give a pictorial representation of the permeability field for the base case with the mesh discretization visible and invisible, respectively. Using the labelling scheme

used by Dawe and Grattoni [10], the quadrant model block $K1$, $K2$, $K3$ and $K4$ are top left, bottom left, top right and bottom right, respectively.

As already mentioned, four upscaled permeability field models were obtained from the high-resolution (*i.e.,* the BaseCase) permeability field. When compared to the BaseCase model, all the upscaled models were upgridded to reduce the resolution of the permeability field (Fig. 2). The first two upscaled models are arithmetic and harmonic averaging methods (referred to as ArithMean and HarmMean, respectively).

In both sets of test-cases, averages are calculated for each block using the 1600 data points from the blocks of the BaseCase to obtain a permeability value for each block in the upscaled models. This effectively homogenizes the permeability field in each block. The upscaled permeability field for the third and fourth cases are referred to as PDFCase and SVDCase, respectively. And, as can be deduced from the names, these cases are based on probability density function (PDF) and SVD, respectively. The description for these permeability field models are presented in Sections 5.1.2 and 5.1.3 respectively. It is appropriate to note that although these models (PDFCase and SVDCase) are upscaled, they retain heterogeneity within the blocks.

5.1.1. BaseCase Pre-processing Algorithm

1. A function is used to randomly generate uniform (*i.e.,* Gaussian) dataset for each block. The range for each block is as below:
   a) **K1** : $700 - 900$ mD
   b) **K2** : $50 - 150$ mD
   c) **K3** : $100 - 200$ mD
   d) **K4** : $1000 - 1200$ mD
2. The number of data points generated for each block is 1600 and the data values are randomly allocated within each block in a structured pattern. Albeit, the simulation mesh is unstructured.
3. Merge the dataset from different blocks into a single file retaining the original "structured pattern" (in step 1 above) for the randomly positioned dataset for each block. This file will be used by the CVFEM-based flow simulator to prescribe the permeability field for the base case.

5.1.2. PDFCase Pre-processing Algorithm

1. The datasets from step one of the pre-processing algorithm for the base case (Section 5.1.1) are used to calculate mean and standard deviation for each block of the permeability field.

2. A function which generates a Gaussian dataset using arithmetic mean and standard deviation is used to stochastically produce a quarter of the data points from the BaseCase for each of the four blocks (*i.e.,* 400 data points for each block).
3. The data values in the dataset for each block is randomly positioned within each block in a structured pattern. As in the base case, the simulation grid is unstructured.
4. Finally, the structured/arranged dataset from each block is combined into a single file and then used by the flow simulator, which merge the permeability mapping to the mesh with the appropriate element-pairs.

5.1.3. SVDCase Pre-processing Algorithm

1. The permeability field obtained in step 3 of the pre-processing algorithm for the base case is factorized using SVD to obtain $\mathbf{U}, \Sigma$, and $\mathbf{V}$.
2. A selected number (z) of singular values are retained in decreasing order of magnitude to form a new diagonal matrix, Σ_{new}.
3. The first z columns of $\mathbf{U}$ and $\mathbf{V}$ are selected to form new truncated matrices call $\mathbf{U_{new}}$ and $\mathbf{V_{new}}$ respectively.
4. Within each column of $\mathbf{U_{new}}$ and $\mathbf{V_{new}}$, a linear interpolation is performed to form a new column with the number of data points in each column reduced to half of the original column. These new columns are recombined to form $\mathbf{U_{new2}}$ and $\mathbf{V_{new2}}$.
5. The permeability field used for the SVD case is the matrix $\mathbf{A_{new2}}$, which is defined as the product of $\mathbf{U_{new2}}\mathbf{\Sigma_{new}}\mathbf{V^T_{new2}}$. It is a permeability field with a quarter of the data values in the base case and therefore a permeability field with reduced order.

5.2. Simulations

For the simulations, each of the model's domain is initially fully saturated with a fluid (Phase 2), and a wetting phase (1) fluid is driven into the domain from the left hand side at a constant mass flow rate. No-flux boundary conditions were imposed on the upper and lower borders of each domain, while mixed fluids are recovered from the right-hand face of the domain. Relative permeability, $\mathcal{K}_{r\alpha}$ (Eqn. 1), which is often expressed as a function of local, residual and maximum phase saturations prescribed in the pore rock matrix. In the simulations conducted for this work, the modified Brooks and

Corey [4] model was used [2],

$$\mathcal{K}_{rw}\left(S_w\right) = \mathcal{K}^{\circ}_{rw}\left[\frac{S_w - S_{w,irr}}{1 - S_{w,irr} - S_{nw,r}}\right]^{n_w}, \tag{7}$$

$$\mathcal{K}_{rnw}\left(S_{nw}\right) = \mathcal{K}^{\circ}_{rnw}\left[\frac{S_{nw} - S_{nw,r}}{1 - S_{w,irr} - S_{nw,r}}\right]^{n_{nw}}, \tag{8}$$

where subscripts w and nw stand for wetting and non-wetting phases, respectively. $\mathcal{K}^{\circ}_{rw}$ and $\mathcal{K}^{\circ}_{rnw}$ are end-point relative permeability to wetting and non-wetting phases, $S_{w,irr}$ and $S_{nw,r}$ are irreducible wetting and residual non-wetting phase saturations, respectively. Exponents n_w and n_{nw} are both set to 2.

Figure 3 shows permeability mapping for all cases, while Figs. 4-8 show phase saturation distribution during fluid injection for time,

$$t = 0.15,\ 0.30,\ 0.50,\ 1.15,\ 1.75 \text{ and } 2.95 \text{ s for all cases.}$$

6. Results and Discussion

Mesh resolution for the the BaseCase and upscaled cases are shown in Fig, 2. Domain of the BaseCase (*i.e.,* high-resolution mesh) was discretised with 4112 P_1DG-P_1 triangular element-pairs, whilst in upscaled cases the domain was discretised with 728 P_1DG-P_1 triangular element-pairs. Therefore the resolution for the upscaled cases is reduced by a factor of approximately 5.6.

Figure 3 compares the permeability distribution for all the models. As indicated in the figure's caption, the permeability legend in Fig. 3(a) is representative for all the other figures (*i.e.,* Fig. 3(b) to (f)). Additionally, Fig. 3(b) to (f) show the cases without the element edges which discretize the domain.

This highlights the fact that the permeability distribution of the ArithMean and HarmMean cases, Fig. 3(c) and (d), are homogeneous within each block, while PDFCase and SVDCase cases, Fig. 3(e) and (f), are heterogeneous. Given that the BaseCase is also heterogeneous, it can be stated that the model for the PDFCase and the SVDCase give a better representation of the BaseCase. An additional consequence of the homogeneity in the ArithMeanCase and the HarmMeanCase is that the upgrid size has no influence on the outcome of their permeability distribution. Whereas, for the PDFCase

and the SVDCase, the permeability field will change if the upgrid resolution changes.

With respect to the PDFCase and for this specific resolution, it is important to note that Fig. 3(e) is only one realiztion of infinitely many possible representations of the PDFCase. Meanwhile, the SVDCase will retain this specific (*i.e.,* Fig. 3(e)) permeability field for this specific resolution (*i.e.,* if linear interpolation is used, but this digresses from the main point and will be discussed in future work). Therefore, the permeability value at a specific point in the PDFCase is not directly related to the data value at the nearest point in the BaseCase because the randomly generated PDF dataset is also randomly arranged within each block. However, the data value at a point in the SVDCase is directly related to the nearest data values with respect to the same point in the BaseCase, throught the interpolation which takes place in the PCS.

Furthermore, prior to the pre-processing required for evaluating the ArithMeanCase, HarmMeanCase and the PDFCase it is necessary to have an understanding of the whole domain and pre-define blocks with similar properties (*i.e.,* blocks $K1$, $K2$, $K3$ and $K4$) in this case. However, with the SVDCase, knowledge of blocks with similar properties is not required prior to the upscaling. Albeit, one has to select the upgrid resolution carefully, if the resolution is too large then there is the risk of losing relevant data in the interpolation. The limits of the techniques used for the SVDCase will be discussed in the author's future work.

Before going on to review the results of the simulations, it is beneficial to briefly consider the Buckley-Leverett and cross-flow behaviour which are be used to validate the results from this work.

Buckley and Leverett [5] in 1942 derived the Buckley-Leverett equation, an analytical (albeit simplified) two phase flow equation. The equation determined that a plane of constant saturation progresses uniformly through the domain during the flow simulation. The equation is referred to as "simplified" because of the assumptions made while deriving it, some of which were ignored in this work. Principally, this work ignores the fact that the equation deals with injection into an homogeneous permeability field while this work deals injection into two blocks ($K1$ and $K2$) with different permeabilities. Additionally, the permeability field in each block is heterogeneous. However, the general validation test or expectation from Buckley-Leverett's influence on this work, is that, the injected fluid saturation in $K1$ and $K2$ is expected to have a piston-shape front within those blocks, subject some

inconsistency at the boundary between the two blocks, and also within the blocks due to the heterogeneity.

Dawe and Grattoni [10] conducted experiments to investigate cross-flow, and as previously mentioned, the permeability field for the experimental work were somewhat replicated here for the simulations. Therefore, the work of Dawe and Grattoni [10] can be used to validate the resulting simulations from this work. In particular, it will be noted that the simulations matches the experiment at the boundary between $K1$ and $K2$. Additionally, the cross-flow from $K1$ to $K4$ is well represented in the simulations.

Figures 4-8 show snapshots of phase 1 (*i.e.,* injected or displacing fluid) saturation field for all studied cases. In Figs. 4-8(a) and (b), even though fluid is injected at the same rate across the left face it travels faster in $K1$ compared to $K2$. Figures 4-8 (c) show that fluid experience a resistance to flow at the interface between $K1$ and $K3$ which encourages the flow into $K4$ (Figs. 4-8 (d) and (e)). Figures 4-8 (f) indicates preferential flow in $K4$ compared to $K3$.

Figure 9 compares phase 1 saturation distribution for all the cases at $t = 1.15s$. Generally, saturation distribution for all cases closely resemble each other with arithmetic and harmonic mean (Figs. 9(b) and (c)) being the most identical. Albeit, closer inspection will reveal that there is more displacement in Fig. 9(b) compared to (c). This is logical giving that the block mean values calculated for arithmetic mean is higher than that for harmonic mean. However, the important feature of Figs. 9(b) and (c) is that they poorly represent the BaseCase (Fig. 9(a)) at the top left hand corner of block $K2$.

Figure 9(d) also shows an inconsistency with the BaseCase (Fig. 9(a)) where it shows phase 1 moving from block $K2$ into $K4$. This inconsistency is with respect to this realization of the PDFCase. Hence, SVDCase in Fig. 9(e) give the best representation of the BaseCase in *i.e.,* Fig. 9(a)

7. Conclusion

Upscaling is a form of model order reduction, and a method of implementing upscaling using singular value decomposition, SVD, is introduced in this work. The SVD method of upscaling first factorizes the matrix of the permeability field and then performs interpolation within the principal component space. The interpolated data in the principal component space is then recombined to form a reduced matrix of the permeability field.

Results show that the permeability field data reduction can be specifically defined for the PDFCase and the SVDCase but not for the ArithMeanCase and the HarmMeanCase. This is because the latter cases will produce the same permeabiBuckleylity field irrespective of the upgrid resolution. The SVDCase is the only technique that does not require a prior knowledge of blocks with similar permeability values before upscaling.

The author's future work will provide a statistical analysis of the technique used for the SVDcase and also presents other implementations of the technique.

References

[1] Adam, A., Pavlidis, D., Percival, J., Salinas, P., Xie, Z., Fang, F., Muggeridge, A., Jackson, M., 2016. Higher-order conservative interpolation between control-volume meshes: Application to advection and multiphase flow problems with dynamic mesh adaptivity. Journal of Computational Physics 321, 512–531.

[2] Alpak, F., Lake, L., Embid, S., 1999. Validation of a modified carman-kozeny equation to model two-phase relative permeabilities. In: SPE Annual Technical Conference and Exhibition. SPE, Texas, SPE56479.

[3] Aziz, K., Settari, A., 1986. Fundamentals of reservoir simulation. Elsevier Applied Science Publishers, New York.

[4] Brooks, R., Corey, A., 1964. Hydrology Papers. Vol. 3. Colorado State University Press, Ch. Hydraulic properties of porous media.

[5] Buckley, S., Leverett, M., 1942. Mechanism of fluid displacement in sands. Transactions of the American Institute of Mining 146, 107–116.

[6] Cardwell, W.T., J., Parsons, R., Dec 1945. Average permeabilities of heterogeneous oil sands. Society of Petroleum Engineers SPE-945034-G (160(1)), 34–42.
URL https://doi.org/10.2118/945034-G

[7] Chen, Z., Huan, G., Ma, Y., 2006. Computational Methods for Multiphase Flows in Porous Media. SIAM.

[8] Christie, M., Blunt, M., 2001. Tenth spe comparative solution project: A comparison of upscaling techniques. Society of Petroleum Engineers SPE-66599-MS.

[9] Christou, K., Randunz, W., Lashore, B., Oliveira, F., Gomes, J., 2018. Numerical investigation of viscous flow instabilities in multiphase heterogeneous porous media. Advances in Water Resources (Submitted).

[10] Dawe, R., Grattoni, C., 2008. Experimental displacement patterns in a 2 x 2 quadrant block with permeability and wettability heterogeneities - problems for numerical modelling. Transport in Porous Media 71, 5–22.

[11] Ewing, R. E., 1997. Aspects of upscaling in simulation of flow in porous media. Advances in Water Resources 20 (5), 349 – 358.
URL http://www.sciencedirect.com/science/article/pii/S0309170896000528

[12] Feldmann, P., Freund, R. W., May 1995. Efficient linear circuit analysis by pade approximation via the lanczos process. IEEE Transactions on Computer-Aided Design of Integrated Circuits and Systems 14 (5), 639–649.

[13] Geiger, S., Roberts, S., Matthäi, S., Zoppou, C., A. Burri, A., 2004. Combining finite element and finite volume methods for efficient multiphase flow simulations in highly heterogeneous and structurally complex geologic media. Geofluids 4 (4), 284–299.

[14] GLOVER, K., 1984. All optimal hankel-norm approximations of linear multivariable systems and their l, -error bounds. International Journal of Control 39 (6), 1115–1193.
URL https://doi.org/10.1080/00207178408933239

[15] Golub, G. H., Reinsch, C., Apr 1970. Singular value decomposition and least squares solutions. Numerische Mathematik 14 (5), 403–420.
URL https://doi.org/10.1007/BF02163027

[16] Gomes, J., Pavlidis, D., Salinas, P., Percival, J., Melnikova, Y., Pain, C., Jackson, M., 2017. A force-balanced control volume finite element method for multi-phase porous media flow modelling. International Journal For Numerical Methods in Fluids 83, 431–445.

[17] Guilleminot, J., Soize, C., Ghanem., R., 2012. Stochastic representation for anisotropic permeability tensor random field. International Journal for Numerical and Analytical Methods in Geomechanics 36(13), 1592–1608.

[18] Hastings, J., Muggeridge, A., 2001. Upscaling uncertainity permeability using small cell renormalization. Mathematical Geology 33(4), 491–502.

[19] Helmig, R., Miller, C., Jakobs, H., Class, H., Hilpert, M., Kees, C., Niessner, J., 2004. Multiphase flow and transport modeling in heterogeneous porous media. In: Bucchianico, A., Mattheij, R., Peletier, M.

(Eds.), Mathematics in Industry 8. Vol. 8 of Water Flow. The European Consortium For Mathemetics in Industry, Springer, pp. 449–488.

[20] Hotelling, H., 1933. Analysis of a complex of statistical variables into principal components. Journal of Educational Psychology 24 (6), 417–441.
URL https://doi.org/10.1037/h0071325

[21] Indelman, P., Dagan, D., 1993. Upscaling of permeability of anisotropic heterogeneous formations - 2 general structure and small perturbation analysis. Water Resources Research 29(4), 925–933.

[22] Jackson, M., Gomes, J., Mostaghimi, P., Percival, J., Tollit, B., Pavlidis, D., Pain, C., El-Sheikh, A., Muggeridge, A., Blunt, M., 2013. Reservoir modeling for flow simulation using surfaces, adaptive unstructured meshes, and control-volume-finite-element methods. In: SPE Reservoir Simulation Symposium.

[23] King, P. R., Jun 1996. Upscaling permeability: Error analysis for renormalization. Transport in Porous Media 23 (3), 337–354.
URL https://doi.org/10.1007/BF00167102

[24] Miller, C., Christakos, G., Imhoff, P., McBride, J., Pedit, J., 1998. Multiphase flow and transport modeling in heterogeneous porous media: Challenges and approaches. Advances in Water Resources 21(2), 77–120.

[25] Moore, B., February 1981. Principal component analysis in linear systems: Controllability, observability, and model reduction. IEEE Transactions on Automatic Control 26 (1), 17–32.

[26] Odabasioglu, A., Celik, M., Pileggi, L. T., Aug 1998. Prima: passive reduced-order interconnect macromodeling algorithm. IEEE Transactions on Computer-Aided Design of Integrated Circuits and Systems 17 (8), 645–654.

[27] Pavlidis, D., Gomes, J., Xie, Z., Percival, J., Pain, C., Matar, O., 2014. Compressive-advection and multi-component methods for interface-capturing. Journal of Computational Physics. In Press.

[28] Pavlidis, D., Gomes, J., Xie, Z., Percival, J., Pain, C., Matar, O., 2016. Compressive advection and multi-component methods for interface-capturing. International Journal for Numerical Methods in Fluids 80 (4), 256–282.

[29] Pillage, L. T., Rohrer, R. A., Apr 1990. Asymptotic waveform evaluation for timing analysis. IEEE Transactions on Computer-Aided Design of Integrated Circuits and Systems 9 (4), 352–366.

[30] Ravalec-Dupin, M. L., 2010. Pilot block method methodology to calibrate stochastic permeability fields to dynamic data. International Association for Mathematical Geosciences 42, 165–185.

[31] Renard, P., de Marsily, G., 1997. Calculating equivalent permeability: A review. Advances in Water Resources 20(5-6), 253–278.

[32] Salinas, P., Pavlidis, D., Xie, Z., Osman, H., Pain, C., Jackson, M., 2018. A discontinuous control volume finite element method for multiphase flow in heterogeneous porous media. Journal of Computational Physics 352, 602–614.

[33] Salinas, P., Percival, J., Pavlidis, D., Xie, Z., Gomes, J., Pain, C., Jackson, M., et al., 2015. A discontinuous overlapping control volume finite element method for multi-phase porous media flow using dynamic unstructured mesh optimization. In: SPE-173279-MS, Reservoir Simulation Symposium. Society of Petroleum Engineers.

[34] Schilders, W., 2008. Introduction to Model Order Reduction. Springer Berlin Heidelberg, Berlin, Heidelberg, pp. 3–32.
URL https://doi.org/10.1007/978-3-540-78841-6_1

[35] Sirovich, L., Oct. 1987. Turbulence and the dynamics of coherent structures. I - Coherent structures. II - Symmetries and transformations. III - Dynamics and scaling. Quarterly of Applied Mathematics 45, 561–571.

[36] Szymkiewicz, A., 2013. Modelling Water Flow in Unsaturated Porous Media. Springer.

[37] Vereecken, H., Kasteel, R., Vanderborght, J., Harter, T., 2007. Upscaling hydraulic properties and soil water flow processes in heterogeneous soils: A review. Vadose Zone Journal 6, 1–28.

[38] Verwoerd, W., 2009. New stochastic model for dispersion in heterogeneous porous media: 1 application to unbounded domains. Applied Mathematical Modelling 33, 605–625.

[39] Wen, X., Gómez-Hernández, J., 1996. Upscaling hydraulic conductivities in heterogeneous media: An overview. Journal of Hydrology 183, ix–xxxii.

[40] Yeo, I.-W., Zimmerman, R. W., Oct 2001. Accuracy of the renormalization method for computing effective conductivities of heterogeneous media. Transport in Porous Media 45 (1), 129–138.
URL https://doi.org/10.1023/A:1011849804979

List of Figures

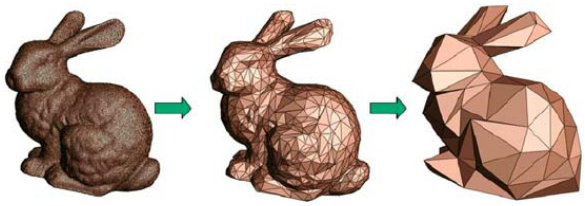

Figure 1: Graphical illustration of model order reduction (initially used by Schilders [34], with graphics credited to Harvard University, Microsoft Research.)

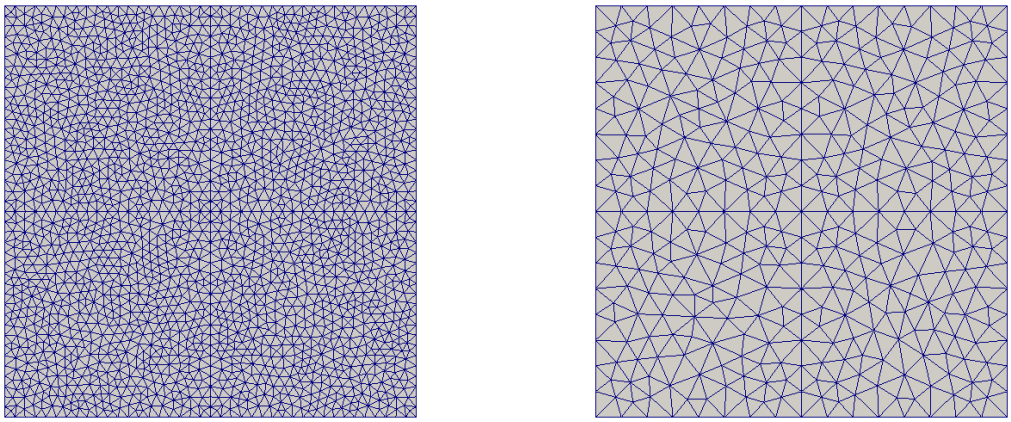

(a) High Resolution Grid (BaseCase) (b) Low Resolution Grid (Upscaled Cases)

Figure 2: Mesh grid used in the performed numerical simulations: (a) high-resolution and (b) upscaled cases with 4112 and 728 triangular elements respectively

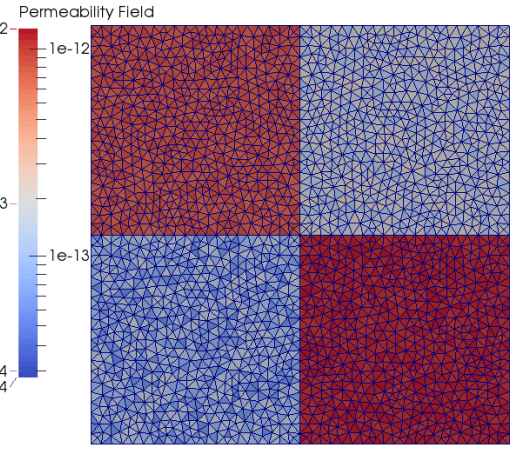

a) BaseCase (overlapped with the mesh)

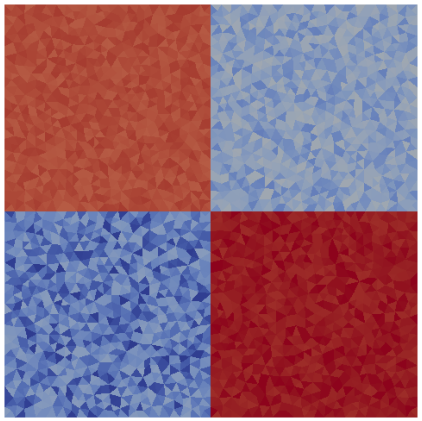

(b) BaseCase (without Mesh)

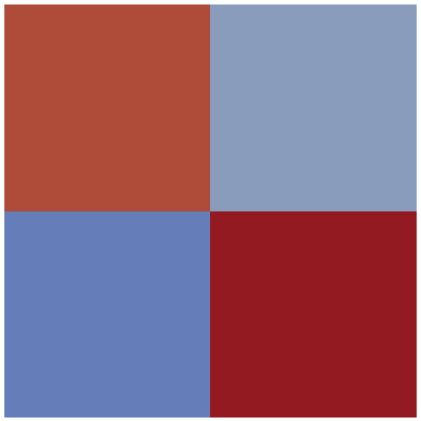

(c) ArithMean Case

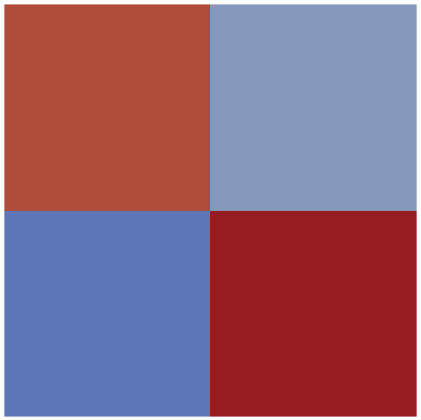

(d) HarmMean Case

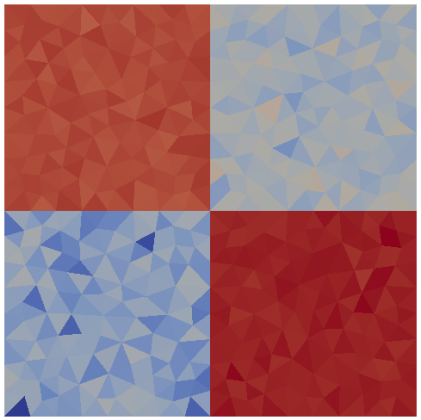

(e) PDFCase

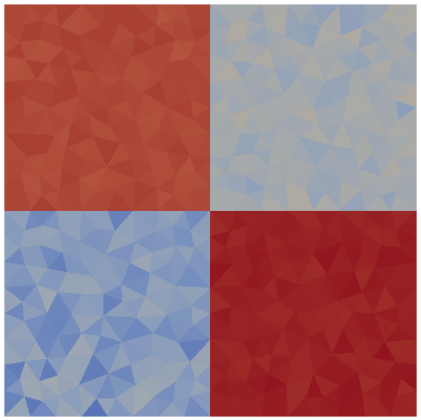

(f) SVDCase

e 3: Permeability field for the base case as well as the upscaled cases (Permeability legend in Fig. 3(a) is representative l the other figures - *i.e.,* Fig. 3(b) to (f))

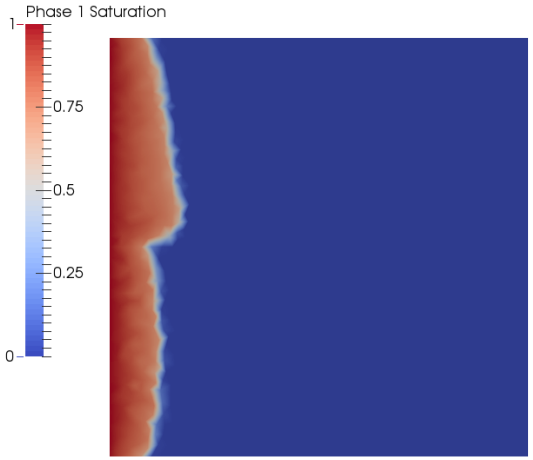

(a) Phase 1 Saturation at t=0.15s

(b) t=0.30s

(c) t=0.50s

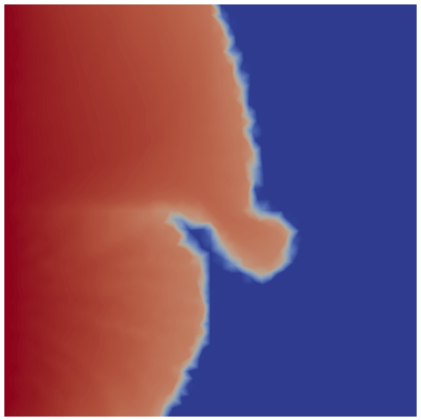

(d) t=1.15s

(e) t=1.75s

(f) t=2.95s

Figure 4: Simulations for the BaseCase (Saturation legend in Fig. 4(a) is representative for all the other figures - *i.e.*, Fig. 4(b) to (f))

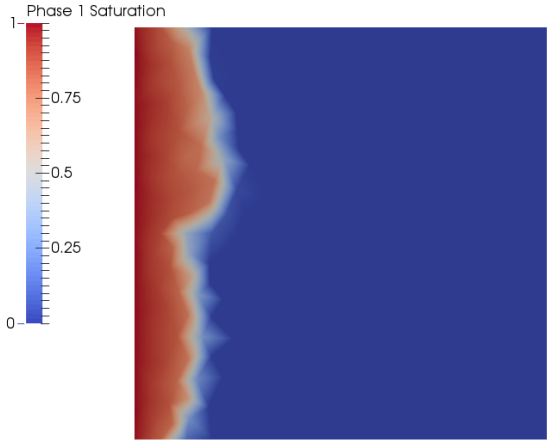

(a) Phase 1 Saturation at t=0.15s

(b) t=0.30s

(c) t=0.50s

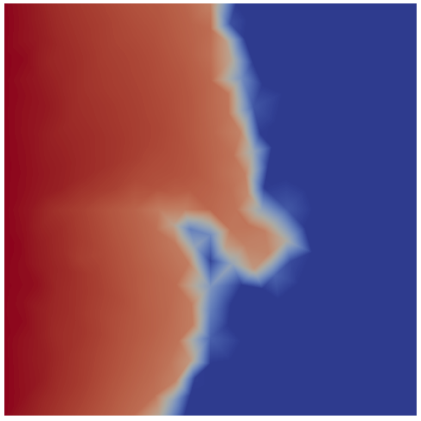

(d) t=1.15s

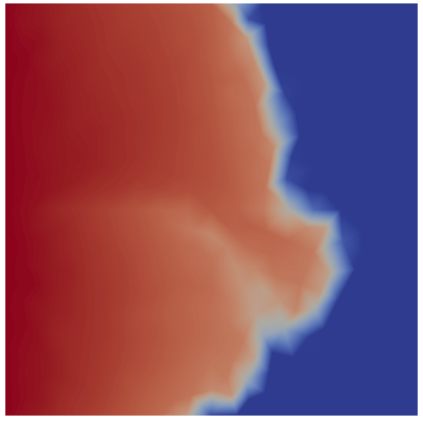

(e) t=1.75s

(f) t=2.95s

Figure 5: Simulations for the ArithMean Case (Saturation legend in Fig. 5(a) is representative for all the other figures - *i.e.*, Fig. 5(b) to (f))

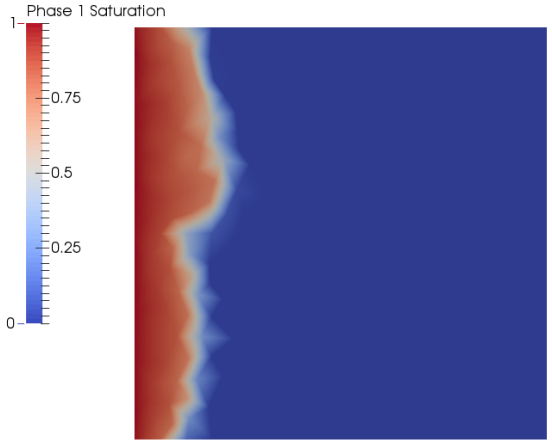

(a) Phase 1 Saturation at t=0.15s

(b) t=0.30s

(c) t=0.50s

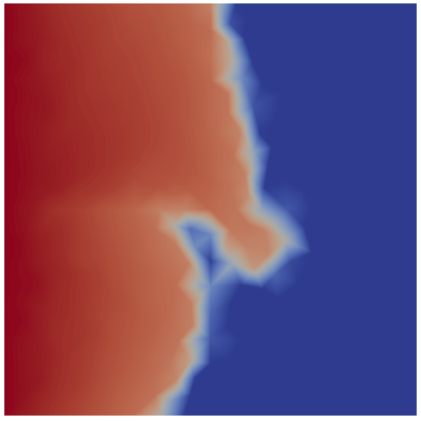

(d) t=1.15s

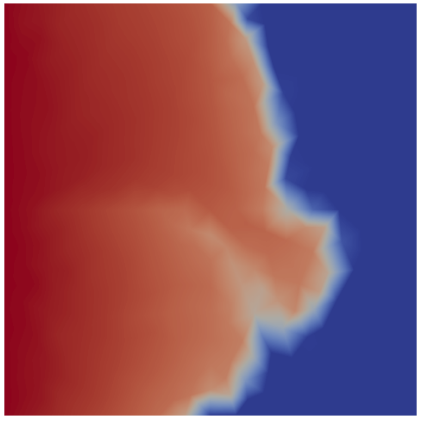

(e) t=1.75s

(f) t=2.95s

Figure 6: Simulations for the HarmMean Case (Saturation legend in Fig. 6(a) is representative for all the other figures - *i.e.*, Fig. 6(b) to (f))

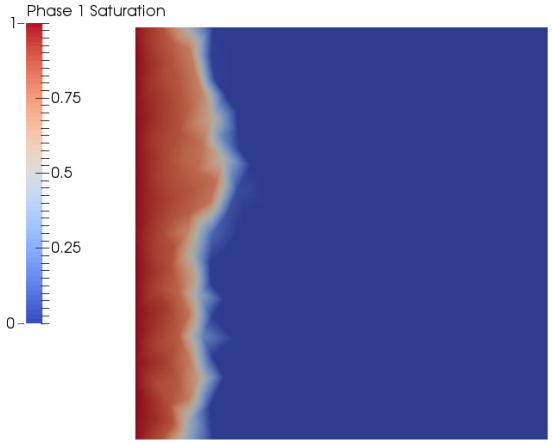

(a) Phase 1 Saturation at t=0.15s

(b) t=0.30s

(c) t=0.50s

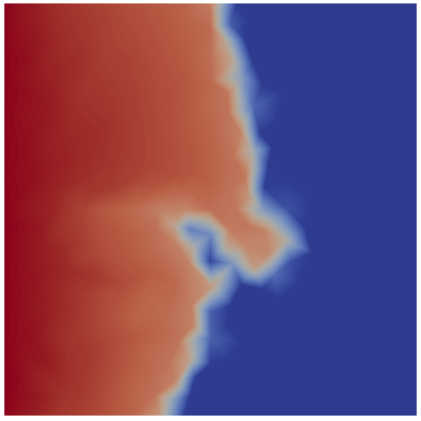

(d) t=1.15s

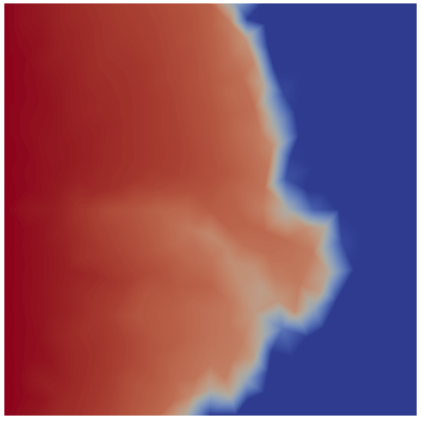

(e) t=1.75s

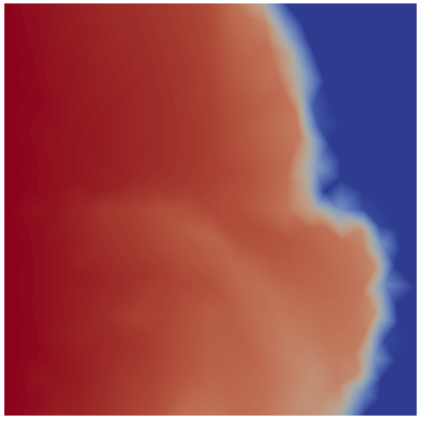

(f) t=2.95s

Figure 7: Simulations for the PDFCase (Saturation legend in Fig. 7(a) is representative for all the other figures - *i.e.*, Fig. 7(b) to (f))

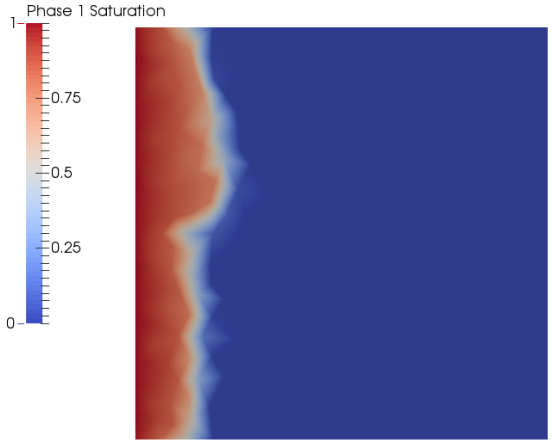

(a) Phase 1 Saturation at t=0.15s

(b) t=0.30s

(c) t=0.50s

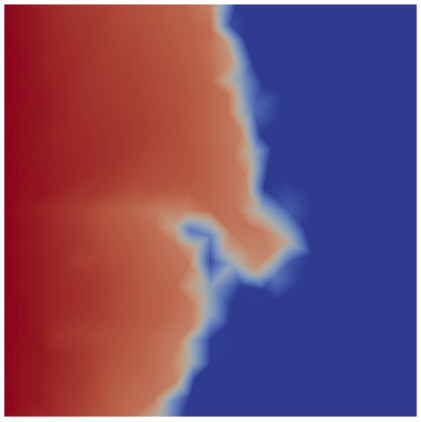

(d) t=1.15s

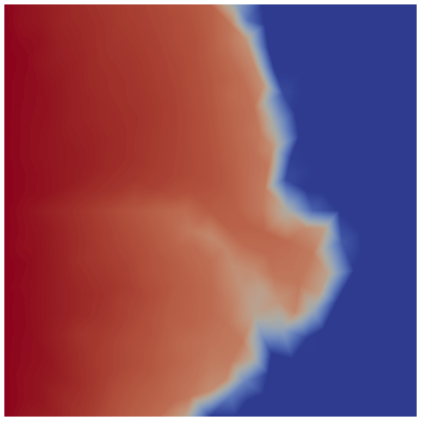

(e) t=1.75s

(f) t=2.95s

Figure 8: Simulation for the SVDCase (Saturation legend in Fig. 8(a) is representative for all the other figures - *i.e.*, Fig. 8(b) to (f))

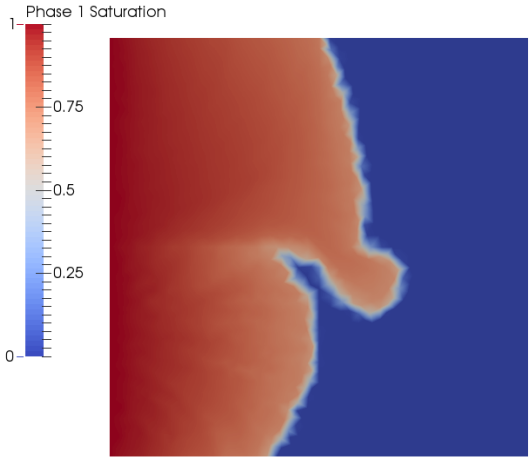

(a) BaseCase

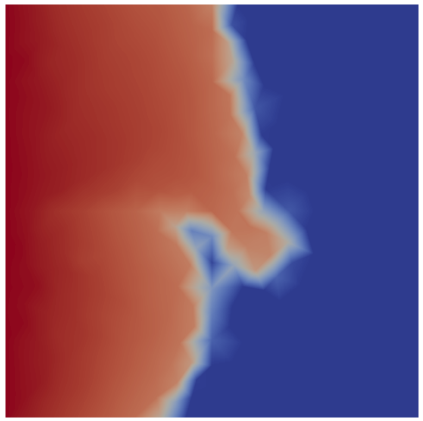

(b) ArithMeanCase

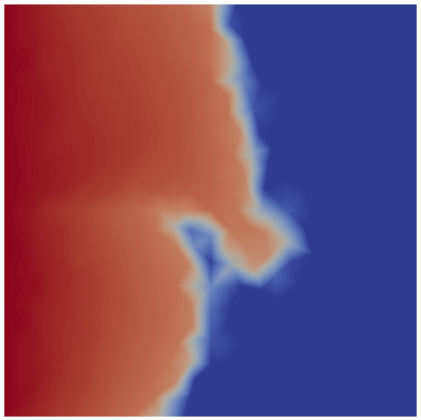

(c) HarmMeanCase

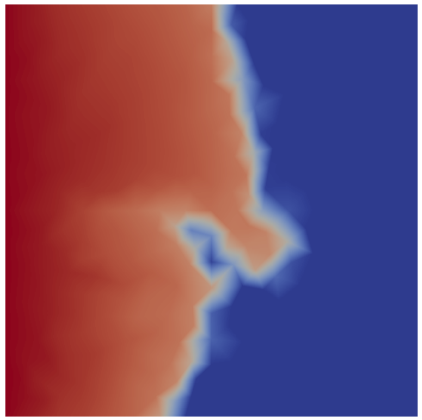

(d) PDFCase

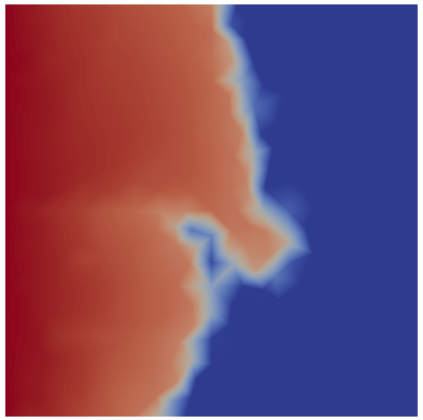

(e) SVDCase

Figure 9: Comparing phase 1 saturation distribution for all the models at $t = 1.15$ s (Saturation legend in Fig. 9(a) is representative for all the other figures - *i.e.*, Fig. 9(b) to (e))